Pergamon

J. Mech. Phys. Solids, Vol. 43, No. 8, pp. 1175–1198, 1995

0022–5096/95 $9.50 + 0.00

0022–5096(95)00033–X

THERMAL CONDUCTIVITY AND EXPANSION OF CROSS-PLY COMPOSITES WITH MATRIX CRACKS

T. J. LU and J. W. HUTCHINSON

Division of Applied Sciences, Harvard University, Cambridge, MA 02138, U.S.A.

(*Received* 2 *December* 1994; *in revised form* 10 *March* 1995)

ABSTRACT

Theoretical models are developed for heat conduction and thermal expansion in a fiber-reinforced ceramic cross-ply laminate containing an array of parallel transverse matrix cracks. Two stages of the transverse matrix cracks are considered: Stage-I with tunnel cracks in the 90° plies aligned parallel to the fibers, and Stage-II with cracks extended across both the 90 and 0° plies with intact fibers bridging the matrix in the 0° plies. The effect of debonded fiber–matrix interfaces in the 0° plies is also considered in Stage-II. Approximate closed form solutions for the overall in-plane thermal conductivities and coefficients of thermal expansion (CTEs) as functions of matrix crack spacing and constituent properties are obtained using an approach which combines an analysis akin to a shear-lag analysis with finite element results. Emphasis is placed on the important class of composites whose fiber expansivity is smaller than that of the matrix. For this class, matrix cracking and interfacial debonding results in reduced thermal expansivity. Interfacial debonding has a significant effect on both longitudinal conductivity and thermal expansivity, especially the latter. Comparisons between the present model predictions and numerical and experimental results are provided where these are available.

1. INTRODUCTION

Explicit approximate expressions are presented in this paper for the overall thermal conductivities and effective coefficients of thermal expansion of a laminated, fiber-reinforced cross-ply ceramic-matrix composite (CMC) as influenced by the two transverse matrix crack systems previewed in Fig. 1. The overall properties are linked to the fundamental properties of the fiber, matrix and interface. In Fig. 1(a) the cross-ply laminate is weakened by a multitude of transverse matrix cracks of uniform spacing d which span the entire cross-section of the 90° plies. These are termed Stage-I matrix cracks. They form as cracks which tunnel in the z-direction perpendicular to an applied tension acting in the y-direction. The composite is fully cracked when the matrix cracks of Fig. 1(a) spread into and across the adjacent 0° plies, as shown in Fig. 1(b). For a cross-ply composite to be effective, these Stage-II cracks must form without breaking the fibers, leaving the fibers to bridge the matrix cracks in the 0° plies. For CMCs with relatively low debond energies, matrix cracking in the 0° plies is usually accompanied by debonding and sliding along the fiber–matrix interfaces.

An important class of CMCs has fibers whose coefficient of thermal expansion is less than that of the matrix. The individual plies and the laminated cross-ply are processed at temperatures in excess of the temperature at which the material will be

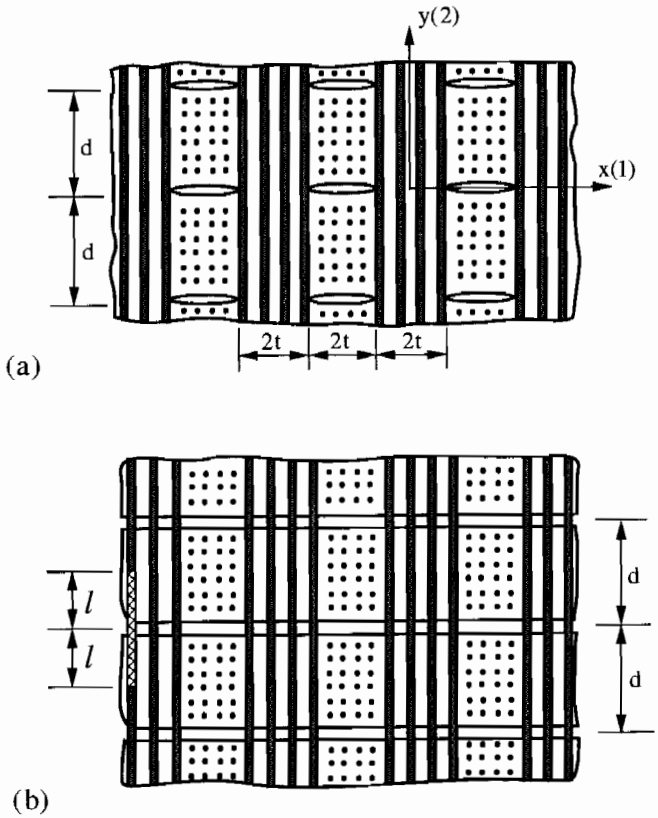

Fig. 1. A fiber-reinforced cross-ply laminate with (a) Stage-I matrix cracks ; and (b) Stage-II matrix cracks.

used. The CTE mismatch between the fiber and matrix affects the behavior of the composite at two scales. Within each ply, the fiber experiences a residual compression along its axis, the matrix is in tension parallel to the fibers, while the fiber–matrix interface is subject to a residual compression. At the scale of the individual plies, the mismatch results in an average residual tensile stress acting across the 90° plies in the y-direction in Fig. 1, and an average residual compressive stress in that same direction in the 0° plies. At the scale of the fiber within the 0° plies, the residual stresses promote matrix cracking without fiber breakage, and, when debonding occurs, the residual stresses tend to keep the interfaces closed. At the larger scale of the plies, the residual tension in the 90° plies in the y-direction adds to an applied tension in that direction to produce conditions which favor the spread of the Stage-I tunnel cracks. At higher applied tension, Stage-II cracks spread across the 0° plies. This sequence of events has been observed in SiC–CAS cross-plies loaded in tension parallel to one of the fiber directions by Beyerle *et al.* (1992). It has been analyzed by Xia and Hutchinson (1994).

Inspired by the first systematic study of Stage-I matrix cracks by Garrett and Bailey (1977), there has been considerable research effort devoted to the description of their effects on stiffness reduction of laminated composite materials. A collection of some

important papers on the subject, both theoretical and experimental, can be found in Laws and Dvorak (1988) and McCartney (1992). More recent works in this area have been directed towards understanding the overall stress–strain behavior of cracked composite laminates as influenced by the constituent properties (Xia *et al.*, 1993; Xia and Hutchinson, 1994; Evans *et al.*, 1994). The effective CTEs of a cross-ply laminate in the presence of Stage-I cracks have been calculated by Bowles (1984) and Adams and Herakovich (1984), using a finite element procedure, and by Hashin (1988) on the basis of variational methods. Herakovich *et al.* (1988), Nairn (1989), McCartney (1992) and Gudmundson and Zang (1993) also discuss some aspects of effects of Stage-I cracks on thermal expansion, especially where they follow from a direct analog to effects on stiffness reduction.

The study in this paper has been motivated by the effort to develop CMCs for structural applications involving high temperatures and high temperature gradients where at least a limited amount of matrix cracking in the vicinity of notches, holes or other sources of stress concentrations must be contemplated for designs to be efficient. The work reported here should be regarded as a continuation of two earlier papers (Lu and Hutchinson, 1995a,b), which focused on some of the same phenomena for unidirectional fiber-reinforced composites. For simplicity, the laminated cross-plies studied here are taken to have an equal number of 0 and 90° plies, each with thickness $2t$. The results presented can be easily adapted to cover laminates with unequal number, and unequal thicknesses, of 0 and 90° plies. For materials whose fibers have a smaller CTE than their matrix, the longitudinal (parallel to the fibers) and transverse CTEs of an undamaged single ply, α_L and α_T, respectively, are ordered according to $\alpha_L < \alpha_T$, causing the Stage-I matrix cracks to remain open in the absence of applied stress. As is customary now in the analysis of fiber-reinforced composite materials, the fibers are taken to be transversely isotropic (elastic moduli, CTEs and thermal conductivities), while the matrix is assumed to be isotropic.

In the sections to follow, the problems for the cross-ply containing either Stage-I or Stage-II cracks will be solved by an approach combining modified shear-lag and finite element analyses. (For brevity of terminology, the method for solving for the overall thermal conductivity will also be referred as a "shear-lag analysis", owing to the mathematical analogy between elasticity and heat conduction.) The explicit expressions thus obtained for the overall thermal conductivities and effective CTEs contain complete information needed for connecting to the constituent material properties, even though the expressions are relatively simple. The accuracy of the solutions will be checked against theoretical predictions and experimental data available in the literature, as well as with some known limiting values when the crack spacing d diminishes to zero.

2. PRELIMINARY CONSIDERATIONS

2.1. *Heat conduction laws*

2.1.1. *Single ply.* Let k_f and γk_f be the longitudinal and transverse thermal conductivities of the fiber, and k_m be the thermal conductivity of the isotropic matrix.

The longitudinal and transverse conductivities k_L and k_T of a crack-free single ply are given by

$$\left.\begin{aligned} k_L &= \rho k_f + (1-\rho)k_m \\ k_T &= \frac{\gamma k_f(1+\rho)+k_m(1-\rho)}{\gamma k_f(1-\rho)+k_m(1+\rho)}k_m \end{aligned}\right\}, \tag{2.1}$$

where ρ is the fiber volume fraction. The rule of mixtures shown above for k_L is exact. The approximate expression for k_T is obtained via an effective-medium approach analogous to the well-known self-consistent method (Christensen, 1979). It is valid for values of ρ up to about 0.6 (Markworth, 1993). Written in rectangular Cartesian coordinates (x, y, z) with the y-axis parallel to the fibers in the 0° plies [Fig. 1(a)], the heat fluxes (energy per unit area per unit time) in an undamaged 0° ply are related to the temperature gradients by Fourier's law as

$$-q_x = k_T T_{,x}, \quad -q_y = k_L T_{,y}, \quad -q_z = k_T T_{,z}, \tag{2.2}$$

where (q_x, q_y, q_z) are the components of the flux vector, $T_{,x} \equiv \partial T/\partial x$, etc. The same relations apply to an undamaged 90° ply with due regard for the change in fiber orientation.

2.1.2. *Cross-ply laminate.* Fourier's law of heat conduction in a crack-free cross-ply laminate reads

$$-q_x = k_x^0 T_{,x}, \quad -q_y = k_y^0 T_{,y}, \quad -q_z = k_z^0 T_{,z}, \tag{2.3}$$

where a quantity with superscript "0" will be used to denote a result where matrix cracking is absent. Throughout the paper, we shall, for convenience, use "thickness" (or "out-of-plane"), "longitudinal" and "transverse" to label laminate properties along x, y and z directions, respectively. In terms of ply conductivities, the overall thermal conductivities of the uncracked laminate are given by

$$k_x^0 = k_T, \quad k_y^0 = k_z^0 = \tfrac{1}{2}(k_L + k_T). \tag{2.4}$$

In the presence of matrix cracking, the overall thermal conductivities of the cross-ply laminate, (k_x, k_y, k_z), are defined by

$$-\bar{q}_x = k_x \bar{T}_{,x}, \quad -\bar{q}_y = k_y \bar{T}_{,y}, \quad -\bar{q}_z = k_z \bar{T}_{,z}, \tag{2.5}$$

where $\bar{q}_i$ and $\bar{T}_{,i}$ $(i = x, y, z)$ represent separately the heat flux intensities and temperature gradients averaged over the cross-ply.

2.2. *Stress–strain laws*

2.2.1. *Single ply.* In the Cartesian coordinates previously defined, the stress–strain law for a transversely isotropic, defect-free 0° ply takes the form

$$\left.\begin{aligned}
\varepsilon_{xx} &= \frac{1}{E_T}\sigma_{xx} - \frac{\nu_L}{E_L}\sigma_{yy} - \frac{\nu_T}{E_T}\sigma_{zz} + \alpha_T \Delta T \\
\varepsilon_{yy} &= -\frac{\nu_L}{E_L}\sigma_{xx} + \frac{1}{E_L}\sigma_{yy} - \frac{\nu_L}{E_L}\sigma_{zz} + \alpha_L \Delta T \\
\varepsilon_{zz} &= -\frac{\nu_T}{E_T}\sigma_{xx} - \frac{\nu_L}{E_L}\sigma_{yy} + \frac{1}{E_T}\sigma_{zz} + \alpha_T \Delta T \\
\varepsilon_{xy} &= \frac{1}{2\mu_T}\sigma_{xy}, \varepsilon_{yz} = \frac{1}{2\mu_T}\sigma_{yz}, \varepsilon_{xz} = \frac{1}{2\mu_L}\sigma_{xz}
\end{aligned}\right\}, \tag{2.6}$$

where, again, the longitudinal and transverse properties of the ply are distinguished by subscripts "L" and "T", and ΔT is a temperature change measured from some conveniently chosen reference temperature. Here, $\mu_T = E_T/2(1+\nu_T)$, but, in general, $\mu_L \neq E_L/2(1+\nu_L)$. With due regard for the two orientations, these relations also hold for an uncracked 90° ply. Throughout the paper identical Poisson ratios for the fiber and matrix are adopted such that $\nu_L = \nu_T = \nu$ ($= \nu_f = \nu_m$). The accuracy of our end results is quite insensitive to this assumption, but the algebraic simplification achieved makes it worthwhile.

The analysis of the effective CTEs requires knowledge of the in-plane moduli of the ply in terms of fiber and matrix properties. The expressions employed here are (Whitney, 1967):

$$\left.\begin{aligned}
E_T &= \frac{(E_f/E_m + 2\eta) + 2\rho(E_f/E_m - \eta)}{(E_f/E_m + 2\eta) - \rho(E_f/E_m - \eta)} E_m \\
E_L &= \rho E_f + (1-\rho) E_m \\
\mu_L &= \frac{\mu_f(1+\rho) + \mu_m(1-\rho)}{\mu_f(1-\rho) + \mu_m(1+\rho)} \mu_m
\end{aligned}\right\}, \tag{2.7}$$

where η is the ratio of axial fiber modulus relative to that in the radial direction. The CTEs of an uncracked single ply, α_L and α_T, have been given by Hashin and Rosen (1965) and later by Lu and Hutchinson (1995a) in a more explicit form for fibers with arbitrary cylindrical anisotropy. For isotropic fibers, they are (Lu and Hutchinson, 1995a)

$$\left.\begin{aligned}
\alpha_L &= \alpha_m + \frac{\rho E_f}{E_L}\Delta\alpha \\
\alpha_T &= \rho\alpha_f + (1-\rho)\alpha_m - \Delta\alpha \frac{\rho(1-\rho)(E_f - E_m)[\nu E_f + (3\nu - 2)E_L]}{E_L[E_f + (1-2\nu)E_L]}
\end{aligned}\right\}, \tag{2.8}$$

where E_f and α_f denote separately the Young's modulus and thermal expansivity of the fiber, and $\Delta\alpha = \alpha_f - \alpha_m$ represents the thermal expansion mismatch. From relations (2.7) and (2.8) one can easily verify that E_L is always larger than E_T if $\eta \geqslant 1$. Moreover, the condition $\alpha_T > \alpha_L$, which ensures that the transverse matrix cracks remain open

even at zero applied stress, is always satisfied if the fiber CTEs do not exceed that of the matrix in magnitude.

2.2.2. *Cross-ply laminate.* Refer to the coordinates defined in Fig. 1, the stress–strain law for an orthotropic, damage-free cross-ply composite reads as

$$\left.\begin{aligned}
\varepsilon_{xx} &= \frac{1}{E_x^0}\sigma_{xx} - \frac{\nu_{xy}^0}{E_y^0}\sigma_{yy} - \frac{\nu_{xz}^0}{E_z^0}\sigma_{zz} + \alpha_x^0 \Delta T \\
\varepsilon_{yy} &= -\frac{\nu_{xy}^0}{E_y^0}\sigma_{xx} + \frac{1}{E_y^0}\sigma_{yy} - \frac{\nu_{yz}^0}{E_z^0}\sigma_{zz} + \alpha_y^0 \Delta T \\
\varepsilon_{zz} &= -\frac{\nu_{xz}^0}{E_z^0}\sigma_{xx} - \frac{\nu_{yz}^0}{E_z^0}\sigma_{yy} + \frac{1}{E_z^0}\sigma_{zz} + \alpha_z^0 \Delta T \\
\varepsilon_{xy} &= \frac{1}{2\mu_{xy}^0}\sigma_{xy}, \varepsilon_{yz} = \frac{1}{2\mu_{yz}^0}\sigma_{yz}, \varepsilon_{xz} = \frac{1}{2\mu_{xz}^0}\sigma_{xz}
\end{aligned}\right\}. \tag{2.9}$$

A conventional analysis based on the assumption that the in-plane strains are identical in every ply of a crack-free cross-ply laminate yields (with equal numbers of plies of each orientation and equal thicknesses assumed)

$$\left.\begin{aligned}
E_x^0 &= E_T, E_y^0 = E_z^0 = \frac{(1+E_L/E_T)^2 - 4\nu_L^2}{2(1+E_L/E_T)(E_L/E_T - \nu_L^2)} E_L \\
\nu_{yz}^0 &= \frac{2\nu_L}{1+E_L/E_T}, \nu_{xy}^0 = \nu_{xz}^0 = \nu_L + \frac{\nu_L^2(1-E_L/E_T)^2}{2(1+E_L/E_T)(E_L/E_T - \nu_L^2)} \\
\mu_{yz}^0 &= \mu_L, \mu_{xy}^0 = \mu_{xz}^0 = \frac{2\mu_L\mu_T}{\mu_L+\mu_T}
\end{aligned}\right\}, \tag{2.10a}$$

and

$$\left.\begin{aligned}
\alpha_x^0 &= \alpha_T - \frac{\nu_L}{1-\nu_L^2 E_T/E_L}\left[\left(1+\nu_L\frac{E_T}{E_L}\right)(\alpha_z^0 - \alpha_T) + (1+\nu_L)(\alpha_y^0 - \alpha_L)\right] \\
\alpha_y^0 &= \alpha_z^0 = \frac{(1-\nu_L)}{2(E_y^0/E_L)(1-\nu_L^2 E_T/E_L)}\left[\alpha_L\left(1+\nu_L\frac{E_T}{E_L}\right) + \alpha_T(1+\nu_L)\frac{E_T}{E_L}\right]
\end{aligned}\right\}. \tag{2.10b}$$

For the most common CMC systems with $\eta > 1$ and $\alpha_f < \alpha_m$, one can see from these relations that

$$E_L > E_y^0 > E_T = E_x^0, \quad \alpha_x^0 \geqslant \alpha_T > \alpha_y^0. \tag{2.11}$$

For CMCs whose fiber properties do not differ significantly from those of the matrix, the above expressions for undamaged laminate properties can be well approximated by

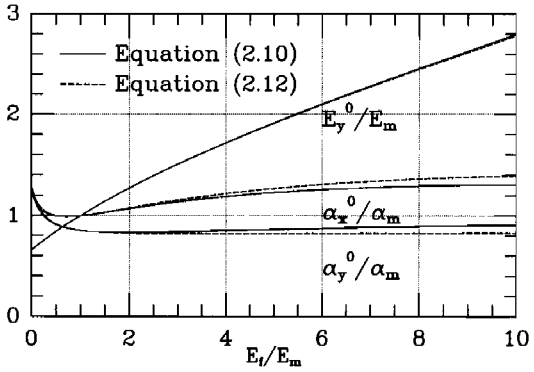

Fig. 2. A comparison between (2.10) and its simplified form (2.12) for the thermoelastic properties of a uncracked cross-ply.

$$E_y^0 = E_z^0 = \tfrac{1}{2}(E_L + E_T), \quad \alpha_x^0 = \alpha_T, \quad \alpha_y^0 = \alpha_z^0 = \frac{\alpha_L E_L + \alpha_T E_T}{E_L + E_T}. \tag{2.12}$$

The error involved with the use of relation (2.12) in lieu of (2.10) is negligible (Fig. 2). At certain places in the sequel, it will be convenient to use these simpler expressions.

With the field variables ($\varepsilon_{ij}, \sigma_{ij}$) replaced by their volume averages ($\bar{\varepsilon}_{ij}, \bar{\sigma}_{ij}$), and the crack-independent laminate properties ($\nu_{ij}^0, E_i^0, \mu_{ij}^0, \alpha_i^0$) replaced by the corresponding effective quantities ($\nu_{ij}, E_i, \mu_{ij}, \alpha_i$), the constitutive relation (2.9) continues to apply in cases where the cross-ply is damaged by matrix cracks aligned perpendicular to the y-axis. Our objective is to explore the extent to which the effective CTEs, α_is ($i = x, y, z$), deviate from their undamaged values, α_i^0s, as a result of matrix cracking and fiber debonding.

3. OVERALL THERMAL CONDUCTIVITIES

3.1. *Stage-I matrix cracks*

Transverse matrix cracks in the 90° plies do not affect the thermal conductivity of a cross-ply in directions parallel to the cracks. Therefore attention is directed to the effect of the cracks in the 90° plies on the overall thermal conductivity of the cross-ply in the longitudinal direction, i.e. on k_y. Figure 3 displays the doubly periodic geometry of Stage-I in the (x, y)-plane, along with the field equations and boundary and symmetry conditions governing steady-state longitudinal heat flow in the composite. (Extensions of the cracks into the 0° plies are also shown in Fig. 3, but these are present only in Stage-II.) Let q_y^0 be the heat flow in the y-direction averaged across the cross-ply. The geometric symmetry and linearity of the temperature field dictates that the temperature distribution on each of the transverse planes half way between the matrix cracks, such as $y = d/2$ and $y = -d/2$, is independent of the coordinate x. Thus, the overall longitudinal thermal conductivity k_y is defined by

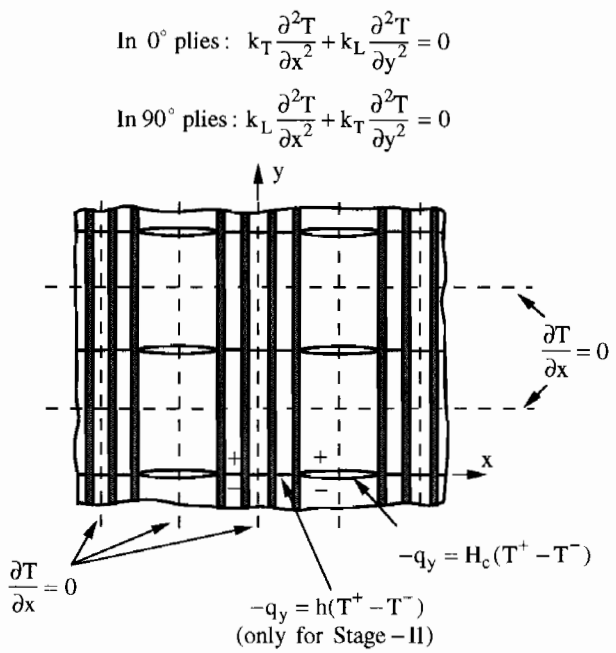

Fig. 3. Field equations, symmetries and boundary conditions for a cracked cross-ply composite.

$$k_y = -\frac{q_y^0}{[T(y = d/2) - T(y = -d/2)]/d}. \tag{3.1}$$

The heat transfer condition across the matrix cracks in the 90° plies is indicated in Fig. 3. At each point along the crack surface, the local heat flow across the crack, $q_y = -k_T \partial T/\partial y$, is taken to be proportional to the temperature jump across the crack according to

$$-q_y = k_T \frac{\partial T}{\partial y} = H_c(T^+ - T^-), \tag{3.2}$$

where H_c is the coefficient of heat transfer and $T^+ - T^- = T(x, 0^+) - T(x, 0^-)$. When the crack does not impede the flow of heat, $H_c = \infty$, while $H_c = 0$ if no heat is transferred, i.e. perfect thermal insulation. Several mechanisms of heat transfer can operate and contribute to H_c, including crack surface contact, gaseous conduction and radiation. In general H_c may be a strong function of temperature. In the analysis, H_c is taken to be a constant independent of T, but in assigning values to H_c a representative average temperature should be used. Discussion of the relative importance of these mechanisms is given in the companion paper by Lu and Hutchinson (1995b).

An approximate analysis of the problem posed in Fig. 3 is given in the Appendix A. The approach closely parallels the analogous shear-lag analysis used in the stress analysis of cracked laminated composites. A similar approach was adopted in the earlier paper dealing with unidirectional fiber-reinforced composites. For the limit in

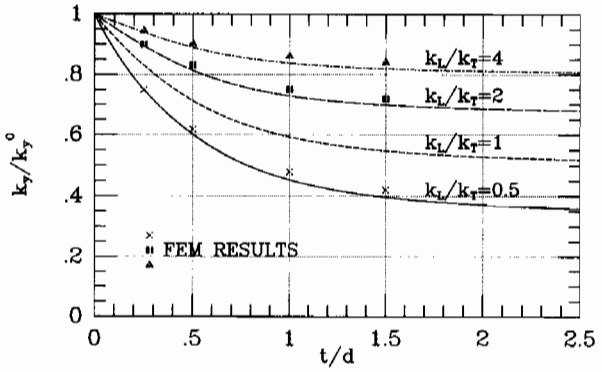

Fig. 4. Model predictions and finite element results for normalized longitudinal thermal conductivity, k_y/k_y^0, of a cross-ply with Stage-I cracks as functions of normalized crack density, t/d, for four selections of conductivity mismatch.

which the Stage-I cracks are perfectly insulating ($H_c = 0$), the longitudinal conductivity is found to be

$$k_y = k_y^0 \left\{ 1 + \frac{k_T}{k_L} \frac{\tanh(m_1 d/2t)}{m_1 d/2t} \right\}^{-1}, \tag{3.3}$$

where $m_1 = (6k_y^0/k_L)^{1/2}$. In the limit $d \to 0$, the conductivity approaches $k_L/2$, corresponding to heat flow only in the 0° plies. From (3.3), curves of k_y/k_y^0 vs normalized crack density, t/d, are displayed in Fig. 4 for four values of k_L/k_T. Also included in the same figure are some numerical results from our finite element analysis of a cell model with the heat transfer boundary conditions posed in Fig. 3. Excellent agreement between the two sets of solutions over the entire range of the crack density parameter is evident.

When H_c is not zero, the analysis in the Appendix A gives

$$k_y = k_y^0 \left\{ 1 + \frac{k_T}{k_L} \frac{\tanh(m_1 d/2t)/(m_1 d/2t)}{1 + (4k_y^0 B_c/m_1 k_T)\tanh(m_1 d/2t)} \right\}^{-1}. \tag{3.4}$$

Here, $B_c = H_c t/k_L$ is the dimensionless Biot number governing the heat transfer across the cracks. Equation (3.4) reduces to (3.3) when $B_c = 0$. The effect of the Biot number on the normalized longitudinal thermal conductivity k_y/k_y^0 is illustrated in Fig. 5 for $k_L/k_T = 2$. (The combination $k_y^0/m_1 k_T$ in (3.4) can be expressed in terms of k_L/k_T). The cracks are nearly perfectly insulating if B_c is less than 0.1; they provide a relatively small barrier to the heat flow when B_c is larger than about 5. Representative values for gaseous conduction of heat across cracks in ceramic materials given in Lu and Hutchinson (1995b) indicate that H_c is inversely proportional to crack opening, whereas B_c is proportional to t. While values of B_c less than 0.1 are possible, one cannot exclude the possibility that they might fall in the range from 0.1 to 5.

3.2. *Stage-II matrix cracks*

The conduction of heat in a CMC cross-ply weakened by Stage-II matrix cracks is impeded by the presence of matrix cracks at two length scales: one characterized by

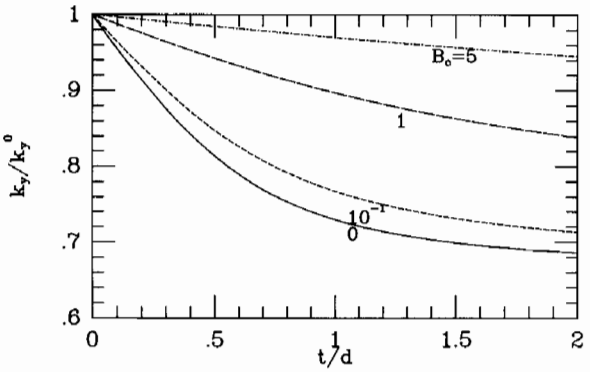

Fig. 5. The effect on the overall longitudinal thermal conductivity of varying the Biot number for Stage-I matrix cracks for $k_L/k_T = 2$.

the Stage-I cracks of length $2t$ in the 90° plies and the other by cracks of length on the order of R_f between the fibers in the 0° plies, where R_f is typically at least one order of magnitude smaller than t. For the composite whose cross-section is depicted in Fig. 3, the bridged matrix cracks in the 0° plies along lines such as $y = 0$ give rise to additional obstruction to the longitudinal flow of heat. In this paper we address two limiting cases for Stage-II cracks: (1) the case in which there is no debonding, and (2) the case in which full debonding in the 0° plies has occurred such that the debond length satisfies $l = d/2$.

3.2.1. *No debonding.* When there is no debonding, the effect of the matrix cracks between the fibers can be represented by an effective thermal impedance, $1/h$, governing the local heat transfer q_y across any point on the line $y = 0$ within the 0° plies. This effective local impedance is defined such that

$$-q_y = h(T^+ - T^-), \tag{3.5}$$

where T^+, as in (3.2), denotes the temperature just above the line of the matrix cracks, with T^- defined similarly for the lower-side. This jump condition will be applied along all crack lines such as $y = 0$ in the 0° plies, as indicated in Fig. 3, where $q_y = -k_L \partial T/\partial y$. The approximate solution given in the Appendix A gives

$$k_y = k_y^I \left(1 + \frac{k_y^I}{hd}\right)^{-1}, \tag{3.6}$$

where now k_y^I denotes the value of k_y given by (3.4) for Stage-I cracks. Note that the result for Stage-I cracks is retrieved as hd/k_y^I becomes large, corresponding to the limit in which the bridged cracks in the 0° plies do not impede the heat flow. Further insight into the parameter hd/k_y^I will emerge below.

The results of Lu and Hutchinson (1995b) for the heat conduction in a unidirectional fiber-reinforced material with widely spaced matrix cracks provide the interface impedance $1/h$. A brief outline of the steps involved in obtaining h is given in the Appendix A. The end result expressed as the nondimensional parameter in (3.6) is

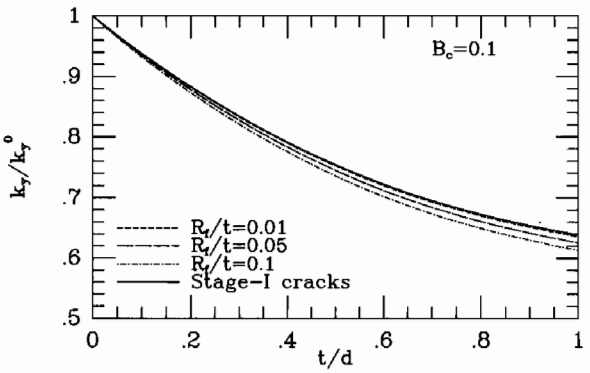

Fig. 6. Effect of fiber radius to half ply thickness ratio R_f/t on the longitudinal thermal conductivity of a perfectly bonded cross-ply in the presence of stage-II matrix cracks. The constitutive parameters used are $B_c = 0.1$, $k_f/k_m = 2$ and $\rho = 0.4$.

$$\frac{hd}{k_y^1} = \frac{\rho k_f k_L}{(1-\rho)k_m k_y^1}\frac{m_2 d}{4R_f}\left\{1+\frac{2k_L^2 B_c R_f}{\rho m_2 k_m k_f t}\right\}, \tag{3.7}$$

where m_2 is another nondimensional parameter given by $m_2 = \{8\gamma k_L/(1-\rho)k_m\}^{1/2}$ and $B_c = H_c t/k_L$ is the Biot number for the cracks in the 0° plies. [The Biot number in Lu and Hutchinson (1995b) is $H_c R_f/k_f$, while the definition of B_c in (3.7) has been taken to be the same as that used in (3.4).] The coefficient of heat transfer H_c for the cracks in the 0° plies need not be the same as for the cracks in the 90° plies. The essential observation which follows from (3.7) is that as long as the matrix crack spacing, d, is large compared to the fiber radius, R_f, the parameter hd/k_y^1 will be large. Thus, by (3.6), the cracks in the 0° plies will have a small effect on k_y. The effect is shown in Fig. 6 for $B_c = 0.1$ for both sets of cracks, $k_f/k_m = 2$ and $\rho = 0.4$. Intuitively, it is easy to understand that the small cracks in the 0° plies are much less effective in impeding the flow of heat than the larger cracks in the 90° plies. The same conclusion applies to the effect of debonding as long as $d \gg l$. The validity of the formula (3.6) breaks down when d becomes comparable to R_f since the derivation of h and its use to prescribe a condition along a crack line in (3.5) tacitly assumes that the two scales involved in the problem are distinct, i.e. d and t are large compared to R_f.

3.2.2. *Fully debonded interfaces in the 0° plies, $l = d/2$.* Extensive debonding of the fiber–matrix interface in the 0° plies can further impede the heat flow by lowering the local conductivity in the x-direction, thereby making it more difficult for the heat to flow around the cracks in the 90° plies. The extreme limit wherein the cracks in both sets of plies have $B_c = 0$ and the fibers in the 0° plies are fully debonded with thermally insulating interfaces ($B_i = 0$) necessarily implies that heat flows only in the fibers such that $k_y = \rho k_f/2$. More generally, the heat conduction problem posed in Fig. 3 for either Stage-I or II cracks applies to the fully debonded case, if one replaces the transverse conductivity k_T in the 0° plies by a value, k_T^*, reflecting the reduced conductivity associated with the interfacial debonding. When this replacement is effected in the analysis given in the Appendix A, the resulting formulas for k_y are identical to those in (3.4) and (3.6), but m_1 must be replaced by

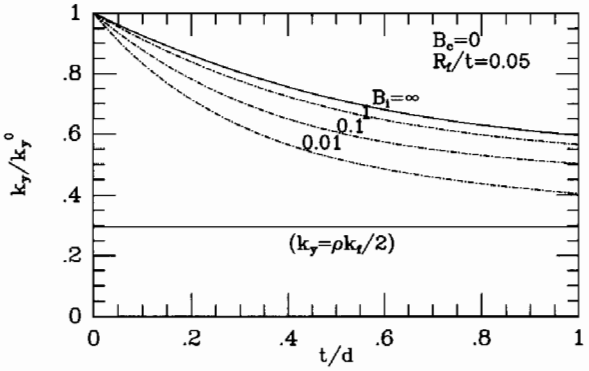

Fig. 7. Effect of fiber–matrix debonding with varying Biot number B_i on the longitudinal CTE of a cross-ply laminate with stage-II matrix cracks for $R_f/t = 0.05$, $B_c = 0$, $k_f/k_m = 2$ and $\rho = 0.4$.

$$m_1^* = \left[\frac{6k_y^0 k_T^*}{k_L k_T}\right]^{1/2}, \tag{3.8}$$

and m_2 must be replaced by

$$m_2^* = \left[\frac{8\gamma k_L}{(1-\rho)k_m}\frac{1}{1+4\gamma/B_i}\right]^{1/2}. \tag{3.9}$$

Here, $B_i = H_i R_f/k_f$ is the Biot number for the debonded fiber–matrix interface with H_i as the coefficient of heat transfer across the debonded interface. Obviously, $m_2^* = 0$ if the debonded interfaces are thermally insulated (i.e. $B_i = 0$) and $m_2^* = m_2$ if the debonded interfaces are perfectly conducting with $B_i = \infty$. An effective media estimate of k_T^* has been derived by Hasselman and Johnson (1987). In the present notation this result is

$$k_T^* = k_m \frac{(1+\gamma/B_i+k_f/k_m)-(1+\gamma/B_i-k_f/k_m)\rho}{(1+\gamma/B_i+k_f/k_m)+(1+\gamma/B_i-k_f/k_m)\rho}. \tag{3.10}$$

The results obtained above are displayed in Fig. 7 to illustrate the role of full fiber–matrix debonding in reducing the longitudinal thermal conductivity. The parameters used to produce the curves are $B_c = 0$ for the cracks in both sets of plies, $R_f/t = 0.05$, $k_f/k_m = 2$ and $\rho = 0.4$. Perfectly insulated Stage-II matrix cracks (i.e. $B_c = 0$) together with fully debonded fiber–matrix interfaces having B_i smaller than about 0.01 serve as major thermal barriers to the longitudinal flow of heat. The approximations invoked in arriving at the modified equations (3.4) and (3.6) do not permit the limit $k_y = \rho k_f/2$ to be retrieved in the limit in which $B_c = B_i = 0$. Judging from the results in Fig. 7, we expect this limit to be highly singular. Intriguing as this limit appears to be, we have not pursued it further. The results shown in Fig. 7 most likely underestimate the reduction in k_y when B_i is very small.

4. EFFECTIVE CTES

4.1. *Stage-I matrix cracks*

For fiber-matrix thermal mismatches such as those discussed in the Introduction, the Stage-I cracks shown in Fig. 1(a) are open as long as the temperature T is below the temperature at which the composite was processed. With ΔT as the temperature change relative to some conveniently chosen reference, the effective coefficients of thermal expansion of the cross-ply are denoted by α_x, α_y, α_z, such that $\alpha_y \Delta T$ denotes the longitudinal strain change due to the temperature change from the reference, and similarly for the other components. The expressions for the CTEs of an uncracked cross-ply are denoted by a superscript "0" and are given in (2.10b) and in a simplified form in (2.12). The overall strain changes in the cracked cross-ply are readily defined. For example, with reference to Fig. 1(a), the displacement component u_y along planes such as $y = \pm d/2$ is independent of x, by symmetry, and therefore $\bar{\varepsilon}_{yy} = (u_y(d/2) - u_y(-d/2))/d$.

It is well-known that one can relate the effect of cracks on the CTEs directly to the increase in compliance due to the cracks. This connection will be exploited here. We also note the close mathematical analogy between the problem for the CTEs and the heat conduction problem considered in Section 3. The expressions for the effect of the cracks on the CTEs turn out to be more complicated than those for the heat conduction coefficients because of Poisson ratio effects. Nevertheless, this close mathematical analogy, together with the parallel analysis for the CTEs of a cracked unidirectional composite (Lu and Hutchinson, 1995a), permits us to omit the somewhat more lengthy details of the shear-lag analysis leading to the expressions given below. Following the presentation of the results, a comparison with results of other authors on the effect of Stage-I cracks will be made.

A necessary starting point in the presentation is the connection between the effect of cracks on compliance change and on change in longitudinal CTE. The change in overall stiffness of the composite with cross-sectional geometry shown in Fig. 1(a) can be written in the form

$$\frac{1}{E_y} = \frac{1}{E_y^0}\left(1 + C_1 \frac{t}{d}\right), \tag{4.3}$$

where C_1 is a dimensionless function of t/d and the dimensionless moduli combinations. Because of the connection between the thermal expansion problem and the compliance problem, one can also express α_y in terms of C_1 as

$$\alpha_y = \alpha_y^0 + C_1 \frac{t}{d} \frac{(1-\nu)E_L(\alpha_L - \alpha_T)}{2E_y^0}. \tag{4.4}$$

The simplified expression for E_y^0 in (2.12) was used in arriving at (4.4), otherwise the connection between (4.3) and (4.4) is exact. Numerical values for C_1 can be obtained from the extensive results in Xia *et al.* (1993) who used a finite element method to compute the compliance change due to Stage-I cracks. The results of the present shear-lag analysis suggest the following approximation for C_1:

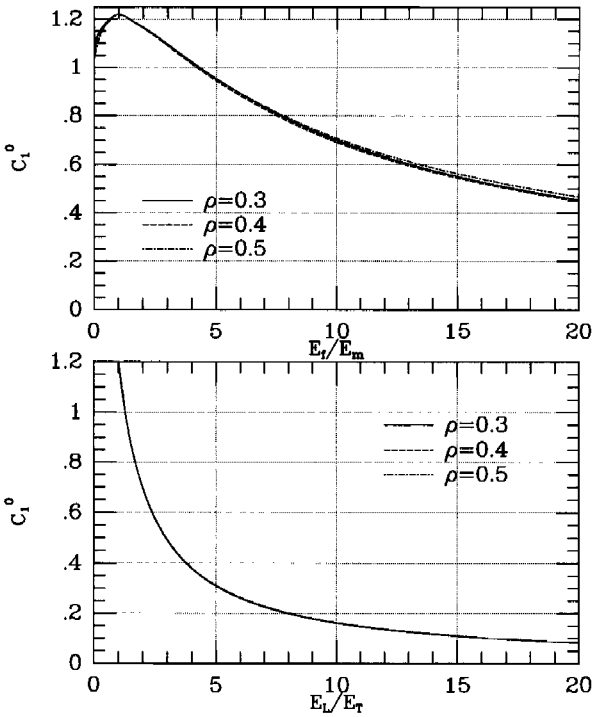

Fig. 8. Numerical results for C_1^0 as function of (a) E_f/E_m ; and (b) E_L/E_T.

$$C_1 = C_1^0 \tanh\left\{\frac{E_T}{C_1^0 E_L}\frac{d}{t}\right\}, \tag{4.5}$$

where C_1^0 must be obtained numerically. From (4.3), C_1^0 can be seen to represent the compliance change when the matrix cracks are widely spaced (i.e. $d > 3t$). The coefficient C_1^0 has been extracted from the numerical results of Xia *et al.* (1993). It depends very weakly on ρ but fairly strongly on E_f/E_m, as can be seen in Fig. 8(a). Here, both the fiber and matrix were taken to be isotropic with $\nu = 0.2$, although the influence of Poisson's ratio on C_1^0 was found to be very small. The results of Fig. 8(a) are replotted as a function of E_L/E_T in Fig. 8(b). For fibers with arbitrary cylindrical anisotropy, one can use (2.7) to calculate E_L/E_T and extract the corresponding C_1^0 from Fig. 8(b).

Approximate expressions for the transverse CTEs, α_x and α_z, can also be derived using an approach such as that given by McCartney (1992). However, because the effect of the cracks on the transverse CTEs is quite small as long as $E_f/E_m < 10$, which is almost always the case for CMCs, we will not present results for the transverse CTEs.

In Fig. 9(a), the effective longitudinal CTE, α_y, for a $[0_2/90_2]_s$ T300/5208 graphite–epoxy cross-ply as a function of the crack density parameter, t/d, is plotted using relation (4.4), where it is compared with the finite element results of Bowles (1984). The effect is large because the longitudinal CTE of the fiber is small compared to the

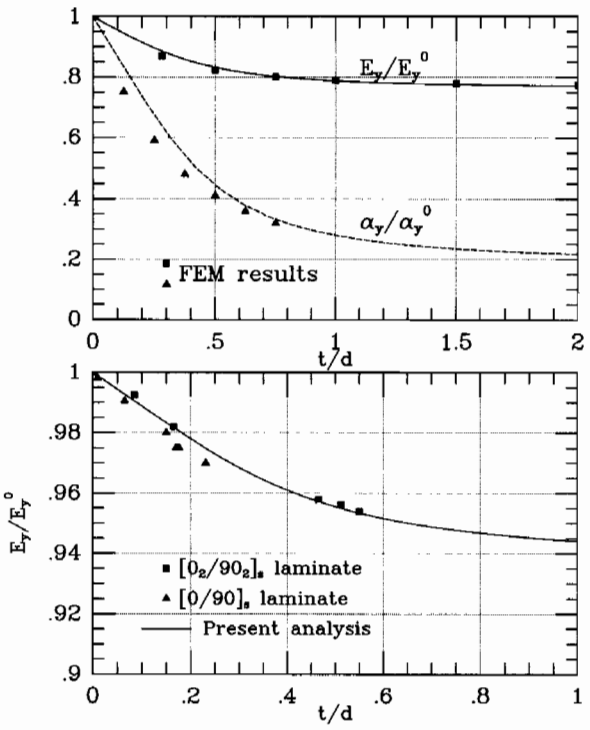

Fig. 9. (a) Model predictions and finite element results for the normalized longitudinal CTE α_y/α_y^0 (Bowles, 1984) and modulus E_y/E_y^0 (Gudmundson and Zang, 1993) for cross-ply laminates with Stage-I matrix cracks ; and (b) Model predictions and experimental data of E_y/E_y^0 (Groves *et al.*, 1987) for cross-ply laminates weakened by Stage-I cracks.

matrix CTE. This is a system in which the anisotropy of the fiber is large so that, instead of (2.8), the equation of Lu and Hutchinson (1995a) for anisotropic fibers was used. Also shown in the same figure is the comparison between relation (4.3) and the finite element analysis of Gudmundson and Zang (1993) for the effective longitudinal Young's modulus of a $[0/90]_s$ glass–epoxy laminate. The constituent properties for each laminate are tabulated in the references cited above. In both cases, close agreement between the present analytical predictions and those from the finite element calculations is demonstrated. Figure 9(b) further illustrates the predictive capability of (4.3) in the light of the experimental measurements of Groves *et al.* (1987) on $[0/90]_s$ and $[0_2/90_2]_s$ Hercules AS4/3502 graphite–epoxy laminates. Again, the analytical results from (4.3) correlate fairly well with the test data. Finally, trends in the variation of α_y are readily generated from (4.4). The ratio α_y/α_y^0 is quite sensitive to variations in either α_T/α_L or E_L/E_T, when all other pertinent parameters are kept unchanged.

The solutions shown in Fig. 9 are typical in that they reveal that α_y (and E_y) has a nearly linear dependence on the normalized crack density, t/d, in the range $d > 3t$, where interactions between neighboring cracks are small. For larger crack densities, interaction increases, the linear dependence of α_y breaks down, and α_y approaches an

asymptotic limit when $d \to 0$. From (4.4) this limiting value of α_y is not α_L but rather $\alpha_L + \nu(\alpha_T - \alpha_L)/(1 + E_L/E_T)$ (to a good approximation), due to a Poisson constraint in the z-direction exerted by the 90° layers on the 0° layers. The 0° plies are not free to undergo unconstrained expansion in the z-direction (governed by α_T) because the 90° plies have a different CTE (i.e. α_L) in the same direction. Since the crack planes in the 90° plies lie parallel to the z-direction, the constraint persists even when the crack density becomes large. The analyses of Hashin (1985, 1988) and Nairn (1989) do not capture this effect. The analyses of these authors predict that α_y should approach α_L as d vanishes. Nairn attributes *ad arbitrium* the discrepancy between this limit and the finite element predictions of Bowles (1984) and Adams and Herakovich (1984) for large crack densities (which, indeed, indicate a limit larger than α_L for the case studied with $\alpha_T > \alpha_L$) to the inability of the finite element analysis to treat highly cracked 90° layers.

4.2. *Stage-II matrix cracks*

4.2.1. *Perfect bonding.* For the Stage-II problem, the matrix cracks in the 0° plies are bridged by the fibers. With σ_{yy} as the local normal stress in the 0° plies just above (and below) the crack plane, the additional displacement in the y-direction arising from the presence of the matrix crack can be represented as a linear "spring" according to

$$\Delta u_y \equiv u_y(x, 0^+) - u_y(x, 0^-) = \frac{D_1^0 R_f}{E_L} \sigma_{yy}. \tag{4.6}$$

The dimensionless coefficient D_1^0, which was computed on the basis of a cylindrical cell model by He *et al.* (1994), is a function of E_f/E_m and ρ, as plotted in Fig. 10. Thus, the model for the Stage-II cracks has the cross-sectional geometry shown in Fig. 1(b). The planes such as $y = 0$, which coincide with the matrix cracks in the 0° plies, are bridged by a continuous distribution of linear springs specified by (4.6). For this model, a connection generalizing that in (4.3) and (4.4) between the compliance and the coefficient of thermal expansion can be obtained. The connection must now reflect the effect of both the cracks in the 90° plies and those in the 0° plies modeled by (4.6).

The shear-lag analysis for the compliance of this model gives

$$\frac{1}{E_y} = \frac{1}{E_y^0}\left[1 + C_1 \frac{t}{d} + 2D_1^0 \frac{E_y^0}{E_L} \frac{R_f}{d}\right], \tag{4.7}$$

with C_1 still given by (4.5). As in the case of the corresponding thermal conductivity problem, the modeling leading to this result is only meaningful when d is large compared to R_f. The connection between the thermal expansion problem and the compliance problem is through the local stresses in the matrix in the 0° plies before cracking occurs. The stress due to an average applied stress $\bar{\sigma}_0$ in the 0° ply is

$$\sigma_m = (1 - a_1\rho)\bar{\sigma}_0/(1 - \rho), \tag{4.8}$$

while the residual stress due to temperature change ΔT is

$$\sigma_m^r = \rho a_2 E_m(\alpha_f - \alpha_m)\Delta T/(1 - \rho), \tag{4.9}$$

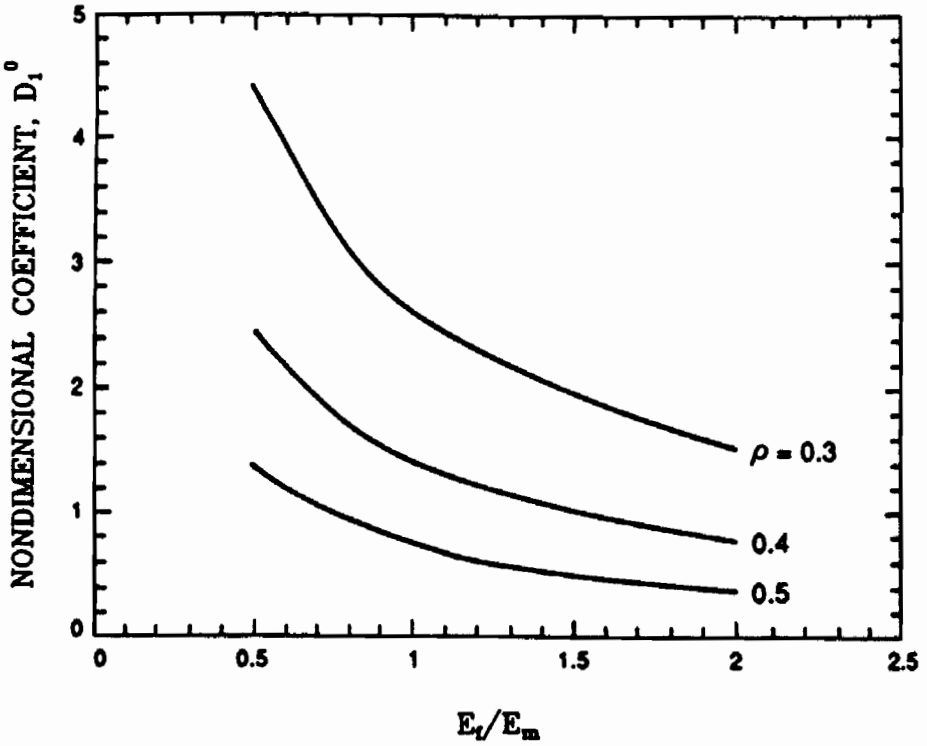

Fig. 10. Numerical results for the nondimensional coefficient D_1^0.

where a_1 and a_2 are two dimensionless functions of ρ and E_f/E_m that are given by Hutchinson and Jensen (1990). For isotropic fibers,

$$a_1 = \frac{E_f}{E_L}, \quad a_2 = \frac{(1-\rho)E_f(E_f+E_L)}{E_L[E_f+(1-2\nu)E_L]}. \tag{4.10}$$

The correspondence between the two problems then gives

$$\alpha_y = \alpha_y^0 + C_1 \frac{t}{d} \frac{(1-\nu)E_L(\alpha_L-\alpha_T)}{2E_y^0} + D_1^0 \frac{R_f}{d} \frac{E_m \rho a_2(\alpha_f-\alpha_m)}{E(1-a_1\rho)}. \tag{4.11}$$

where C_1 and D_1^0 are the same coefficients which appear in (4.7).

An example displaying the effective longitudinal CTE α_y from (4.11) as a function of the normalized crack density t/d is shown in Fig. 11 for $R_f/t = 0.1$, 0.05 and 0.01. In these plots α_y is normalized by α_y^0, and both the fiber and matrix are taken to be isotropic with $\rho = 0.4$, $\nu = 0.2$, $E_f/E_m = 2$ and $\alpha_f/\alpha_m = 0.5$, typical for some CMCs. When the fibers are perfectly bonded to the matrix in the 0° plies, matrix cracking is seen to have only a very small effect on α_y, even when the density of matrix cracks is as large as $d/t = 1$. In other words, assuming debonding does not accompany matrix cracking in the 0° plies, CMCs will experience rather little change in their CTEs. This can be contrasted with the much larger effect on polymer matrix composites seen in

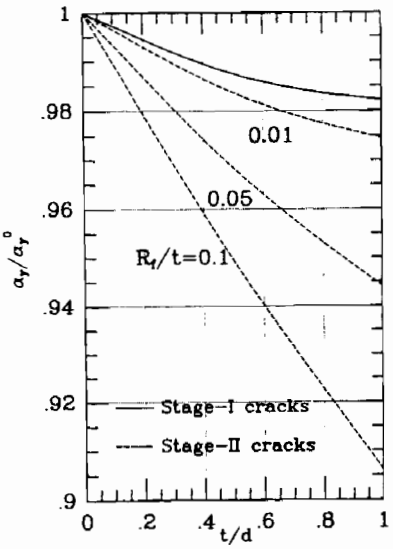

Fig. 11. Effect of fiber radius to half ply thickness ratio R_f/t on the longitudinal CTE of a perfectly bonded cross-ply in the presence of stage-II matrix cracks. The constitutive parameters used are $\rho = 0.4$, $\nu = 0.2$, $E_f/E_m = 2$ and $\alpha_f/\alpha_m = 0.5$.

Fig. 9(a) for a particular carbon fiber composite. The small effect of matrix cracking in the absence of debonding on the CTEs of CMCs can also be contrasted with the appreciable effects on the thermal conductivity of these materials.

4.2.2. *Partially or fully debonded fiber–matrix interface with frictionless sliding.* Debonding and sliding can alter the situation just described. Specifically, it will now be shown that when debonding in the 0° plies occurs, allowing frictionless sliding to take place, the change in α_T can be appreciable. Let l be the length of interface debond extending on either side of each matrix crack surface in the 0° layers [Fig. 1(b)], with $l = 0$ and $l = d/2$ representing, respectively, the cases of no debonding and full debonding. The debonded region of the interface is assumed to have formed previously during the process of matrix cracking and is assumed to remain closed under the conditions that the fiber has a smaller CTE than the matrix.

Relations (4.7) and (4.11) continue to apply for the cross-ply with crack spacing d and debond length l, provided that $l \ll (t, d)$ and that the coefficient D_1^0 is replaced by

$$D_1 = D_1^0 + \frac{(1-\rho)E_m}{\rho E_f}\frac{2l}{R_f}. \tag{4.12}$$

The additional term in this expression is the contribution to the effective "spring constant" in (4.6) (with D_1 replacing D_1^0) arising from the frictionless sliding and stretching of the debonded segments of the fibers. (The expression has been taken from He *et al.* (1994), and further simplified by taking a factor χ in that paper to be unity. In this form it agrees with the most widely used expression for the extra displacement across a bridged crack due to frictionless sliding.) It must be emphasized that the replacement of D_1^0 by D_1 in (4.7) and (4.11) can only be justified when it is

legitimate to model the effect of the debonded fibers as a line-spring, that is when $l \ll (t, d)$.

When the fiber–matrix interfaces are fully debonded ($l = d/2$), the longitudinal CTE of the cross-ply is dominated by the CTE of the fibers in the 0° ply and is weakly dependent on the crack spacing d. Neglecting the Poisson constraint effect exerted by the 90° ply on the expansion of the 0° ply in the z-direction but accounting for the Poisson interaction in the radial direction between the fiber and matrix in the 0° plies, we arrive at (Lu and Hutchinson, 1995a)

$$\alpha_y = \alpha_L + 4a_2\rho^2 c_1^2 \frac{\Delta\alpha}{1-a_1\rho}, \tag{4.13}$$

where the dimensionless coefficient c_1, as a_1 and a_2, was introduced in Hutchinson and Jensen (1990). For isotropic fibers, the laminate CTE α_y becomes

$$\alpha_y = \alpha_L + (\alpha_f - \alpha_m)\frac{(1-\rho)E_m(E_f+E_L)}{E_L(E_f+(1-2\nu)E_L)}. \tag{4.14}$$

It can be readily verified from (2.8) and (4.14) that $\alpha_y = \alpha_f$ if the Poisson ratio $\nu = 0$. In general, α_y is slightly smaller than α_f due to Poisson interaction between the fiber and the matrix. (Recall, again, that the residual stresses are such that the fiber–matrix interface remains closed.) This approximate result does not depend on the matrix crack spacing. Guidance as to how frictional sliding resistance alters these results can be obtained from the study of unidirectional reinforcement in Lu and Hutchinson (1995a).

On the basis of relations (4.11–4.13), curves of α_y/α_y^0 vs t/d are computed and presented in Fig. 12 with $R_f/t = 0.05$ for four values of normalized debond length l/t.

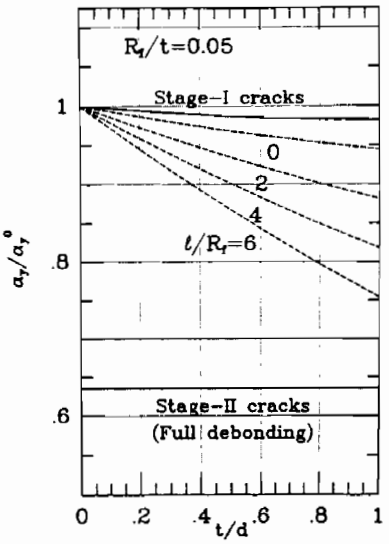

Fig. 12. Effect of frictionless debonding on the longitudinal CTE of a cross-ply laminate with stage-II matrix cracks for $R_f/t = 0.05$. The constitutive parameters used are identical to those listed in Fig. 11.

The same choice of parameters is employed as in Fig. 11, namely $\rho = 0.4$, $\nu = 0.2$, $E_f/E_m = 2$ and $\alpha_f/\alpha_m = 0.5$. Note that the scale of the ordinate is much larger in Fig. 12 than in Fig. 11. Debonding clearly has a major effect on α_y. Also included in Fig. 12 is the prediction from (4.14) for fully debonded stage-II matrix cracking. The value for α_y from (4.14) in this example is 0.88 α_f, which falls below α_f for reasons discussed above.

Finally, we note that the procedures used to estimate the increase of compliance due to matrix cracking in a cross-ply can be applied to calculate the average longitudinal stress acting on the 0° plies when the cracked cross-ply is loaded in the y-direction. An analysis leading to closed form formulas for this average stress quantity is given in Appendix B for both Stage-I and Stage-II matrix cracks. The results obtained can be applied to simulate the stress–strain curves of cross-ply composites in a way described by Evans *et al.* (1994).

5. CONCLUSIONS

The changes in thermal conductivities and coefficients of thermal expansion due to matrix cracking and interfacial debonding in cross-ply CMCs have been analyzed, with emphasis placed on composite systems where the CTE of the matrix is larger than that of the fiber. Realistic densities of Stage-I cracks result in significant reduction in the overall longitudinal thermal conductivity but have a rather small effect on the CTEs of ceramic cross-plies. This is in contrast to the appreciable changes Stage-I cracks produce in the longitudinal CTE of certain polymer–matrix composite systems where the fiber expansivity is much smaller than that of the matrix. When fiber–matrix debonding does not accompany matrix cracking in the 0° plies, Stage-II cracking produces only small incremental changes from Stage-I cracking, as far as the overall conductivities and expansivities are concerned. Debonding and sliding of the fiber–matrix interfaces in the 0° plies produces substantial changes from the Stage-I values. The combination of matrix cracking and interfacial debonding can reduce the longitudinal thermal conductivity k_y and CTE α_y of the cracked cross-ply to levels close to $\rho k_f/2$ and α_f, respectively. The properties of the cross-ply in the other two directions are much less affected by the presence of matrix cracks under the conditions that perfect bonding exists between the fiber and the matrix. Debonding does change the transverse thermal conductivity, but in a manner which is not influenced by the existence of the matrix cracks.

ACKNOWLEDGMENTS

The work reported here was partially supported by the ARPA University Initiative ONR Prime Contract N00014-92-J-1808, and by the Division of Applied Sciences, Harvard University. The commercial ABAQUS finite element code was used in carrying out some of the numerical computations.

REFERENCES

Adams, D. S. and Herakovich, C. T. (1984) Influence of damage on the thermal response of graphite–epoxy laminates. *J. Thermal Stresses* **7**, 91–103.

Beyerle, D. S., Spearing, S. M. and Evans, A. G. (1992) Damage and failure in unidirectional ceramic-matrix composites. *J. Am. Ceram. Soc.* **75,** 3321–3330.
Bowles, D. E. (1984) Effect of microcracks on the thermal expansion of composite laminates. *J. Comp. Mater.* **17,** 173–187.
Christensen, R. M. (1979) *Mechanics of Composite Materials.* Wiley, New York.
Evans, A. G., Domergue, J.-M. and Vagaggini, E. (1994) Methodology for relating the tensile constitutive behavior of ceramic-matrix composites to constituent properties. *J. Am. Ceram. Soc.* **77,** 1425–1435.
Garrett, K. W. and Bailey, J. E. (1977) Multiple transverse fracture in 90° cross-ply laminates of a glass fiber-reinforced polyester. *J. Mater. Sci.* **12,** 157–168.
Groves, S. E., Harris, C. E., Highsmith, A. L., Allen, D. H. and Norvell, R. G. (1987) An experimental and analytical treatment of matrix cracking in cross-ply laminates. *Expl. Mech.* **27,** 73–79.
Gudmundson, P. and Zang, W. (1993) An analytical model for thermoelastic properties of composite laminates containing transverse matrix cracks. *Int. J. Solids Struc.* **30,** 3211–3231.
Hashin, Z. (1985) Analysis of cracked laminates: a variational approach. *Mech. Mater.* **4,** 121–136.
Hashin, Z. (1988) Thermal expansion coefficients of cracked laminates. *Comp. Sci. Tech.* **31,** 247–260.
Hasselman, D. P. H. and Johnson, L. F. (1987) Effective thermal conductivity of composites with interfacial thermal barrier resistance. *J. Comp. Mater.* **21,** 508–514.
He, M. Y., Wu, B.-X., Evans, A. G. and Hutchinson, J. W. (1994) Inelastic strains due to matrix cracking in unidirectional fiber-reinforced composites. *Mech. Mater.* **18,** 213–229.
Herakovich, C. T., Aboudi, J., Lee, S. W. and Strauss, E. A. (1988) Damage in composite laminates: effects of transverse cracks. *Mech. Mater.* **7,** 91–107.
Hutchinson, J. W. and Jensen, H. M. (1990) Models of fiber debonding and pullout in brittle composites with friction. *Mech. Mater.* **9,** 139–163.
Laws, N. and Dvorak, G. J. (1988) Progressive transverse cracking in composite laminates. *J. Comp. Mater.* **22,** 900–916.
Lu, T. J. and Hutchinson, J. W. (1995a) Effect of matrix cracking and interface sliding on the thermal expansion of fiber-reinforced composites. *Composites* **26** (in press).
Lu, T. J. and Hutchinson, J. W. (1995b) Effect of matrix cracking on the overall thermal conductivity of fiber-reinforced composites. *Phil. Trans. Roy. Soc. Lond.* (in press).
McCartney, L. N. (1992) Theory of stress transfer in a 0°–90°–0° cross-ply laminate containing a parallel array of transverse cracks. *J. Mech. Phys. Solids* **40,** 27–68.
Markworth, A. J. (1993) The transverse thermal conductivity of a unidirectional fiber composite with fiber–matrix debonding: a calculation based on effective-medium theory. *J. Mater. Sci. Lett.* **12,** 1487–1489.
Nairn, J. A. (1989) The strain energy release rate of composite microcracking: a variational approach. *J. Comp. Mater.* **23,** 1106–1129.
Whitney, J. M. (1967) Elastic moduli of unidirectional composites with anisotropic filaments. *J. Comp. Mater.* **1,** 188–193.
Xia, Z. C. and Hutchinson, J. W. (1994) Matrix cracking of cross-ply ceramic composites. *Acta Metall. Mater.* **42,** 1933–1945.
Xia, Z. C., Carr, R. R. and Hutchinson, J. W. (1993) Transverse cracking in fiber-reinforced brittle matrix, cross-ply laminates. *Acta Metall. Mater.* **41,** 2365–2376.

APPENDIX A: "SHEAR-LAG" ANALYSIS OF HEAT CONDUCTION IN CROSS-PLY LAMINATES WITH STAGE-I AND STAGE-II MATRIX CRACKS

The analysis presented below for the thermal conductivity of the composite with cross-section shown in Fig. 1 serves to illustrate the approach for the somewhat more complicated

problem for thermal expansion. A "shear-lag" type formulation for the Stage-I problem is presented first. This is extended later to cover the case where Stage-II cracks are present.

The steady-state temperature distribution in the 0° layers, $T_0(x, y)$, must satisfy

$$k_T \frac{\partial^2 T_0}{\partial x^2} + k_L \frac{\partial^2 T_0}{\partial y^2} = 0. \tag{A.1}$$

By symmetry, along the central axes of the representative 0° ply,

$$T_{0,x} = 0, \quad \text{for } x = 0, \tag{A.2a}$$

with a similar condition at the center of the 90° plies

$$T_{90,x} = 0, \quad \text{for } |x| = 2t, \tag{A.2b}$$

where $T_{90}(x, y)$ denotes the distribution of temperature in the 90° layers. For intimate thermal contact at the 0°/90° interfaces,

$$\left.\begin{aligned} T_{0,x} &= T_{90,x}, \\ T_0 &= T_{90}, \end{aligned}\right\} \quad \text{for } |x| = t. \tag{A.3}$$

Introduce the average temperature gradients defined by

$$\hat{T}_{0,y}(y) = \frac{1}{t}\int_0^t T_{0,y}(x, y)\,dx, \quad \hat{T}_{90,y}(y) = \frac{1}{t}\int_t^{2t} T_{90,y}(x, y)\,dx. \tag{A.4}$$

The global heat balance condition satisfied on every cross-section transverse to the plies then reads

$$\tfrac{1}{2}[k_T \hat{T}_{90,y}(y) + k_L \hat{T}_{0,y}(y)] = -q_y^0, \tag{A.5}$$

where q_y^0 is the longitudinal heat flux intensity averaged across the laminate.

Let $T_0^0(y)$ be the temperature at the center of the 0° ply and let $T_0^i(y)$ be the temperature at the 0°/90° interface. The distribution of temperature in the 0° ply is taken to be a quadratic interpolation of the values at the center and edges according to

$$T_0(x, y) = T_0^0(y) + \frac{x^2}{t^2}(T_0^i(y) - T_0^0(y)), \quad \text{for } x < t. \tag{A.6}$$

Integration of the governing differential equation (A.1), with the aid of (A.4), leads exactly to

$$\frac{\partial \hat{T}_{0,y}}{\partial y} = -\frac{k_T}{k_L}\frac{T_{0,x}^i(y)}{t}, \tag{A.7}$$

where $T_{0,x}^i(y) \equiv T_{0,x}(\pm t, y)$ is the transverse temperature gradient at the 0°/90° interface. This gradient can, in turn, be obtained from (A.6) in terms of $T_0(x, y)$ and $T_0^0(y)$. Next, differentiation of (A.7) with respect to y gives

$$\frac{d^2 \hat{T}_{0,y}}{dy^2} = -\frac{2(k_T/k_L)}{t^2}\left(\frac{dT_{90}^i}{y} - \frac{dT_0^0}{y}\right), \tag{A.8}$$

where the condition $T_0^i = T_{90}^i$ has been used. Note also that, with the substitution $T_0^i = T_{90}^i$, a direct averaging of (A.6) yields

$$\frac{d\hat{T}_0}{dy} = \frac{1}{2}\left(\frac{dT_0^0}{dy} + \frac{dT_{90}^i}{dy}\right). \tag{A.9}$$

To further simplify the problem, the transverse variation of the temperature gradient across the 90° ply, $\partial T_{90}/\partial x$, is ignored. Under these conditions, the quantities dT_0^0/dy and dT_{90}^i/dy are readily expressed in terms of $d\hat{T}_0/dy$ on the basis of (A.5) and (A.9). Finally, the governing differential equation (A.8) is reduced to

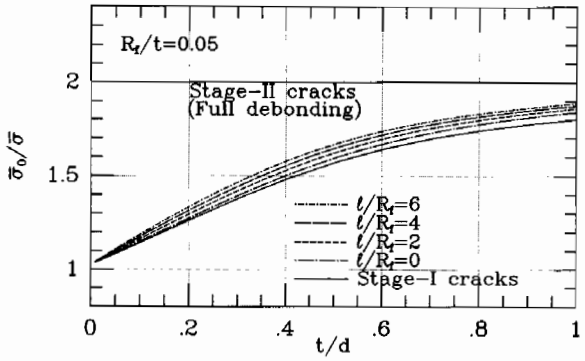

Fig. A1. Effect of fiber matrix debonding with frictionless sliding on the average longitudinal stress $\bar{\sigma}_0$ acting on the 0° ply when a cross-ply laminate with stage-II matrix cracks is loaded by stress $\bar{\sigma}$ in the same direction. The constitutive parameters used are $R_f/t = 0.05$, $\rho = 0.4$, $\nu = 0.2$ and $E_f/E_m = 2$.

APPENDIX B: "STRESS CONCENTRATION" IN 0° PLY DUE TO STAGE-I AND STAGE-II MATRIX CRACKS

The solution given in the text for the increase in compliance of a cross-ply due to transverse matrix cracking is employed here to determine the average longitudinal stress $\bar{\sigma}_0$ sustained by a 0° ply when the cracked cross-ply is loaded by stress $\bar{\sigma}$ in a direction parallel to the fibers of the 0° ply. Given $\bar{\sigma}_0$ as a function of crack spacing and moduli variables, one can simulate the tensile stress–strain behaviors of laminated cross-ply composites using the behavior of the unidirectional material in the 0° plies under the assumption that it is the behavior of these plies which dominates (Evans *et al.*, 1994).

If the cross-ply is uncracked, $\bar{\sigma}_0 = E_L\bar{\sigma}/E_y^0$. For the most common CMCs, $\bar{\sigma}_0$ is only slightly larger than $\bar{\sigma}$ when no matrix cracks are present. As an illustrative example, one has $\bar{\sigma}_0/\bar{\sigma} = 1.05$ if $E_f/E_m = 2$, $\rho = 0.4$ and $\eta = 1$. The "stress concentration factor" $\bar{\sigma}_0/\bar{\sigma}$ increases markedly, however, once matrix cracking (and interfacial debonding) occurs in the cross-ply and approaches 2 in extreme conditions. For a cross-ply weakened by Stage-I cracks, $\bar{\sigma}_0$ is rigorously given by

$$\bar{\sigma}_0 = \bar{\sigma}\frac{E_L}{E_y^0}\left(1 + C_1\frac{t}{d}\right), \tag{B.1}$$

where C_1 has been defined in (4.5). If Stage-II cracks accompanied by debonding and frictionless sliding take place in the cross-ply and if the debond length satisfies the condition $l \ll (t, d)$, $\bar{\sigma}_0$ is well-approximated by

$$\bar{\sigma}_0 = \bar{\sigma}\frac{E_L}{E_y^0}\left(1 + C_1\frac{t}{d} + 2D_1\frac{E_y^0}{E_L}\frac{R_f}{d}\right)\Big/\left(1 + D_1\frac{R_f}{d}\right), \tag{B.2}$$

where D_1 is given by (4.12). When full debonding with frictionless sliding occurs at the fiber–matrix interface ($l = d/2$), the dependence of $\bar{\sigma}_0$ on the crack spacing d is weak. With the Poisson constraining effect exerted by the 90° ply on the deformation of the 0° ply ignored (but not the Poisson interaction between the fiber and matrix in the 0° ply), the load carrying capacity of the cracked cross-ply is due to the 0° plies alone such that $\bar{\sigma}_0 = 2\bar{\sigma}$. Based on relation (B.2), the ratio $\bar{\sigma}_0/\bar{\sigma}$ is depicted in Fig. A1 against the crack density parameter t/d as a function of normalized debond length l/R_f for $R_f/t = 0.05$, $E_f/E_m = 2$, $\eta = 1$, $\rho = 0.4$ and $\nu = 0.2$. It is bounded by $\bar{\sigma}_0/\bar{\sigma} = 2$ for fully debonding and (B.1) for Stage-I cracks, for which the curve is also displayed in Fig. A1. Observe that although the matrix cracks in the 0° plies have negligible effect on $\bar{\sigma}_0/\bar{\sigma}$ when there is perfect bonding between the fiber and matrix, extensive debonding with frictionless sliding have the potential to raise $\bar{\sigma}_0/\bar{\sigma}$ close to the limit 2.

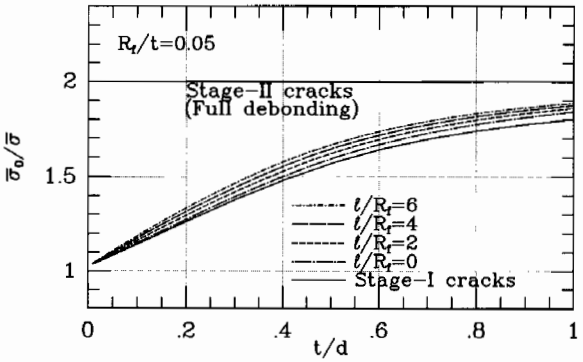

Fig. A1. Effect of fiber–matrix debonding with frictionless sliding on the average longitudinal stress $\bar{\sigma}_0$ acting on the 0° ply when a cross-ply laminate with stage-II matrix cracks is loaded by stress $\bar{\sigma}$ in the same direction. The constitutive parameters used are $R_f/t = 0.05$, $\rho = 0.4$, $\nu = 0.2$ and $E_f/E_m = 2$.

APPENDIX B: "STRESS CONCENTRATION" IN 0° PLY DUE TO STAGE-I AND STAGE-II MATRIX CRACKS

The solution given in the text for the increase in compliance of a cross-ply due to transverse matrix cracking is employed here to determine the average longitudinal stress $\bar{\sigma}_0$ sustained by a 0° ply when the cracked cross-ply is loaded by stress $\bar{\sigma}$ in a direction parallel to the fibers of the 0° ply. Given $\bar{\sigma}_0$ as a function of crack spacing and moduli variables, one can simulate the tensile stress–strain behaviors of laminated cross-ply composites using the behavior of the unidirectional material in the 0° plies under the assumption that it is the behavior of these plies which dominates (Evans *et al.*, 1994).

If the cross-ply is uncracked, $\bar{\sigma}_0 = E_L\bar{\sigma}/E_T^0$. For the most common CMCs, $\bar{\sigma}_0$ is only slightly larger than $\bar{\sigma}$ when no matrix cracks are present. As an illustrative example, one has $\bar{\sigma}_0/\bar{\sigma} = 1.05$ if $E_f/E_m = 2$, $\rho = 0.4$ and $\eta = 1$. The "stress concentration factor" $\bar{\sigma}_0/\bar{\sigma}$ increases markedly, however, once matrix cracking (and interfacial debonding) occurs in the cross-ply and approaches 2 in extreme conditions. For a cross-ply weakened by Stage-I cracks, $\bar{\sigma}_0$ is rigorously given by

$$\bar{\sigma}_0 = \bar{\sigma}\frac{E_L}{E_T^0}\left(1 + C_1\frac{t}{d}\right), \tag{B.1}$$

where C_1 has been defined in (4.5). If Stage-II cracks accompanied by debonding and frictionless sliding take place in the cross-ply and if the debond length satisfies the condition $l \ll (t, d)$, $\bar{\sigma}_0$ is well-approximated by

$$\bar{\sigma}_0 = \bar{\sigma}\frac{E_L}{E_T^0}\left(1 + C_1\frac{t}{d} + 2D_1\frac{E_T^0}{E_L}\frac{R_f}{d}\right)\Big/\left(1 + D_1\frac{R_f}{d}\right), \tag{B.2}$$

where D_1 is given by (4.12). When full debonding with frictionless sliding occurs at the fiber–matrix interface ($l = d/2$), the dependence of $\bar{\sigma}_0$ on the crack spacing d is weak. With the Poisson constraining effect exerted by the 90° ply on the deformation of the 0° ply ignored (but not the Poisson interaction between the fiber and matrix in the 0° ply), the load carrying capacity of the cracked cross-ply is due to the 0° plies alone such that $\bar{\sigma}_0 = 2\bar{\sigma}$. Based on relation (B.2), the ratio $\bar{\sigma}_0/\bar{\sigma}$ is depicted in Fig. A1 against the crack density parameter t/d as a function of normalized debond length l/R_f for $R_f/t = 0.05$, $E_f/E_m = 2$, $\eta = 1$, $\rho = 0.4$ and $\nu = 0.2$. It is bounded by $\bar{\sigma}_0/\bar{\sigma} = 2$ for fully debonding and (B.1) for Stage-I cracks, for which the curve is also displayed in Fig. A1. Observe that although the matrix cracks in the 0° plies have negligible effect on $\bar{\sigma}_0/\bar{\sigma}$ when there is perfect bonding between the fiber and matrix, extensive debonding with frictionless sliding have the potential to raise $\bar{\sigma}_0/\bar{\sigma}$ close to the limit 2.